Inorg. Chem. **2007**, *46*, 6155–6163

Synthesis, Structural Characterization, and Electrophosphorescent Properties of Rhenium(I) Complexes Containing Carrier-Transporting Groups

Zhenjun Si,[†,‡] Jiang Li,[§] Bin Li,*[,†] Feifei Zhao,[§] Shiyong Liu,*[,§] and Wenlian Li[†]

Key Laboratory of Excited State Processes, Changchun Institute of Optics, Fine Mechanics and Physics, and Graduate School of the Chinese Academy of Sciences, Chinese Academy of Sciences, Changchun 130033, P. R. China, and State Key Laboratory of Integrated Optoelectronics, Jilin University, Changchun 130023, P. R. China

Received August 30, 2006

Two novel diimine rhenium(I) carbonyl complexes with the formula $[Re(CO)_3(L)Br]$, where L = 1-(4-5′-phenyl-1,3,4-oxadiazolylbenzyl)-2-pyridinylbenzoimidazole (**1**) and 1-(4-carbazolylbutyl)-2-pyridinylbenzoimidazole (**2**), have been successfully synthesized and characterized by elemental analysis, ^{1}H NMR, and IR spectra. Their electrochemical, photophysical, and electroluminescent behaviors, along with the X-ray crystal structure analysis of **2**, are also described. White electrophosphorescent devices were fabricated using **1** and **2** as emitters. The devices based on carbazole-containing (hole-transporting group) **2** with the structure ITO/*m*-MTDATA (30 nm)/NPB (20 nm)/**2**:CBP (8%, 30 nm)/Bphen (20 nm)/Alq_3 (20 nm)/LiF (0.8 nm)/Al (200 nm) exhibit Commission Internationale de L'Eclairage coordinates of $x = 0.34$, $y = 0.33$ with a maximum brightness of 2300 cd/m^2 at 580 mA/cm^2. When a brightness of 1500 cd/m^2 appears at 230 mA/cm^2, the devices based on 10 wt % **2** still possess 56% of the maximum efficiency which appeared at 2.7 mA/cm^2. These performances are among the best reported for devices using Re(I) complexes as emitters. By comparison of the electroluminescent properties of the devices based on **1** and **2**, we conclude that the introduction of the carbazole group into the ligand improves the performance of **1**-doped devices.

Introduction

Interest in next generation displays and lighting technologies has stimulated research on organic light-emitting devices (OLEDs).[1] Especially, white-emitting OLEDs (WOLEDs) based on phosphorescent materials have seen significant improvement.[2] As a result, d^6 and d^8 transition metal phosphorescent complexes[3−5] have been studied intensively throughout the world. This class of compounds afford high-emission quantum efficiencies (theoretically up to 100%) compared to that of fluorescent materials because of the

* To whom correspondence should be addressed. E-mail: lib020@ciomp.ac.cn (B.Li.); syliu@mail.jlu.edu.cn (S.Liu.). Fax: +86 0431 86176935 (B.Li.).

† Changchun Institute of Optics, Fine Mechanics and Physics.

‡ Graduate School of the Chinese Academy of Sciences.

§ Jilin University.

(1) (a) Tang, C. W.; Vanslyke, S. A. *Appl. Phys. Lett.* **1987**, *51*, 913. (b) Burroughes, J. H.; Bradley, D. D. C.; Brown, A. R.; Mackay, R. N.; Marks, K.; Friend, R. H.; Burns, P. L.; Holmes, A. B. Nature **1990**, *347*, 539. (c) Thompson, M. E.; Forrest, S. R. *Nature* **1998**, *395*, 151. (d) Li, J.; Liu, D.; Li, Y.; Lee, C.-S.; Kwong, H.-L.; Lee, S. *Chem. Mater.* **2005**, *17*, 1208. (e) Lin, B. C.; Cheng, C. P.; You, Z.-Q.; Hsu, C.-P. *J. Am. Chem. Soc.* **2005**, *127*, 66. (f) Wong, K.-T.; Chen, Y.-M.; Lin, Y.-T.; Su, H.-C.; Wu, C.-C. *Org. Lett.* **2005**, *7*, 5361.

(2) (a) Kim, T.-H.; Lee, H. K.; Park, O.; Chin, B. D.; Lee, S.-H.; Kim, J. K. *Adv. Funct. Mater.* **2006**, *16*, 611. (b) Lee, S. K.; Hwang, D.-H.; Jung, B.-J.; Cho, N. S.; Lee, J.; Lee, J.-D.; Shim, H.-K. *Adv. Funct. Mater.* **2005**, *15*, 1647.

(3) (a) Tsutsui, T.; Yang, M.-J.; Yahiro, M.; Nakamura, K.; Watanabe, T.; Tsuji, T.; Fukuda, Y.; Wakimoto, T.; Miyaguchi, S. *Jpn. J. Appl. Phys.* **1999**, *38*, L1502. (b) Baldo, M. A.; Lamansky, S.; Burrows, P. E.; Thompson, M. E.; Forrest, S. R. *Appl. Phys. Lett.* **1999**, *75*, 4. (c) Adachi, C.; Baldo, M. A.; Forrest, S. R.; Thompson, M. E. *Appl. Phys. Lett.* **2000**, *77*, 904. (d) Ostrowski, J. C.; Robinson, M. R.; Heeger, A. J.; Bazan, G. C. *Chem. Commun.* **2002**, 784. (e) Rayabarapu, D. K.; Paulose, B. M. J. S.; Duan, J.-P.; Cheng, C.-H. *Adv. Mater.* **2005**, *17*, 349. (f) Lyu, Y.-Y.; Byun, Y.; Kwon, O.; Han, E.; Jeon, W. S.; Das, R. R.; Char, K. *J. Phys. Chem. B* **2006**, *110*, 10303. (g) Bolink, H. J.; Cappelli, L.; Coronado, E.; Parham, A.; Stössel, P. *Chem. Mater.* **2006**, *18*, 2778.

(4) (a) Ma, Y.; Zhang, H.; Shen, J.; Che, C.-M. *Synth. Met.* **1998**, *94*, 245. (b) Bernhard, S.; Gao, X.; Malliaras, G. G.; Abruna, H. D. *Adv. Mater.* **2002**, *14*, 433. (c) Jiang, X.; Jen, A. K.-Y.; Carlson, B.; Dalton, L. R. *Appl. Phys. Lett.* **2002**, *80*, 713. (d) Gao, F. G.; Bard, A. *J. Chem. Mater.* **2002**, *14*, 3465. (e) Chen, Y.-L.; Lee, S.-W.; Chi, Y.; Hwang, K.-C.; Kumar, S. B.; Hu, Y.-H.; Cheng, Y.-M.; Chou, P.-T.; Peng, S.-M.; Lee, G.-H.; Yeh, S.-J.; Chen, C.-T. *Inorg. Chem.* **2005**, *44*, 4287.

10.1021/ic061645o CCC: $37.00
Published on Web 06/21/2007

strong spin−orbit coupling in the luminescence process. With the aim of further exploring novel phosphorescent materials, several groups paid attention to Re(I) complexes,[6] of which the d^6 electronic configuration is identical to that of the corresponding Os(II) and Ir(III) systems. However, most of the previously reported phosphorescent Re(I) complexes used in the OLEDs have the disadvantage of the saturation of emission sites resulting from triplet−triplet annihilation which leads to low efficiency at high current density.[7] Therefore, it is pressing to explore new Re(I) complexes to overcome the shortcoming mentioned above. Two methods are available to develop novel Re(I) complexes: (i) the application of novel diimine ligands with different ligand field strengths[6d,7b,8] to adjust the molecular orbital energy levels in the Re(I) complexes which are related to the photochemical, photophysical, and electrochemical events and (ii) introduction of functional groups with electro-donating[6c,7c,9] or -accepting[6a,10] properties into diimine ligands, which is helpful to improve the carrier-transporting ability of Re(I) complexes in OLEDs and avoid the triplet−triplet annihilation because of the steric hindrance effect. To date, the first tactic has been successfully employed to obtain electroluminescent (EL) Re(I) complexes without functional groups. But Re(I) complexes containing carrier-transporting groups are rarely used in OLEDs. In this article, we successfully applied the second tactic to design and synthesize two novel Re(I) complexes which contain the electron-transporting moiety 2,5-diphenyl-1,3,4-oxadiazole and the hole-transporting moiety carbazole. The synthesized complexes, [1-(4-5′-phenyl-1,3,4-oxadiazolylbenzyl)-2-pyridinylbenzoimidazole]$Re(CO)_3Br$ (**1**) and [1-(4-carbazolylbutyl)-2-pyridinyl-benzimidazole] $Re(CO)_3Br$ (**2**), are capable of being vacuum deposited to construct EL devices. The optical, electrochemical, thermal, and electroluminescent properties of complexes **1** and **2** are also reported, accompanied by the X-ray crystal structure analysis of **2**.

Experimental Section

Materials. All starting chemicals and charge-transporting materials used in the process of the OLEDs devices fabrication, 4,4′,4″-tris[3-methylphenylphenylamino]triphenylamine (*m*-MTDATA), 4,7-diphenyl-1,10-phenanthroline (Bphen), 4,4′-bis[*N*-(1-naphthyl)-*N*-phenylamino]biphenyl (NPB), 4,4′-dicarbazolyl-1,1′-biphenyl (CBP), tris(8-hydroxy-quinoline)aluminum (Alq_3), and LiF, were commercially available and were used without further purification unless otherwise noted. The organic precursor of 2-4′-methylbenzyl-5-benzyloxadiazole (**a**) was synthesized according to a published method;[11] the ligands of 1-(4-carbazolylbutyl)-2-pyridinylbenzoimidazole (**L1**),[12] 1-(4-5′-Phenyl-1,3,4-oxadiazolylbenzyl)-2-pyridinylbenzoimidazole (**L2**),[13] and the corresponding Re(I) complexes[14] were prepared according to the modified procedures. All reactions and manipulations were carried out under N_2 with the use of standard inert atmosphere and Schlenk techniques. Solvents used for synthesis were dried by standard procedures and stored under N_2. Solvents used in luminescent and electrochemical studies were of spectroscopic and anhydrous grades, respectively.

Synthesis of 2-(4-Bromomethylphenyl)-5-phenyl-1,3,4-oxadiazole (c). Fifteen grams of (0.097 mol) 4-methylbenzoyl chloride was added dropwise to a solution of 13.20 g (0.097 mol) of benzohydrazide, 9.80 g (0.097 mol) of triethylamine, and 150 mL of chloroform at room temperature (RT). The resulting mixture was stirred for 1 h and then filtered. The collected solid was washed with water and methanol to give 23.43 g (yield 95%) of the product *N*′-benzoyl-4-methylbenzohydrazide. A mixture of 20.00 g of *N*′-benzoyl-4-methylbenzohydrazide and 250 mL of $POCl_3$ in a 500 mL flask was refluxed under nitrogen for 5 h. The excessive $POCl_3$ was then distilled out, and the residue was poured into water. The crude solid product was collected by filtration and purified by recrystallization from chloroform/methanol to give 15.80 g of 2-4′-tolyl-5-phenyl-1,3,4-oxadiazole (**a**) as needlelike crystals (85%). A mixture of 14.16 g (0.06 mol) of compound **a**, 11.68 g (0.066 mol) of *N*-bromosuccinimide (NBS), 0.13 g of benzoyl peroxide, and 200 mL of CCl_4 in a 500 mL flask was refluxed for 5 h. The mixture was filtered while it was still hot. The solid was washed with hot chloroform. The residual solid was recrystallized from tetrahydrofuran (THF)/methanol to give 8.00 g of product as white needlelike crystals (40%). ^1H NMR ($CDCl_3$, 500 MHz): δ 4.570 (2H, s), 7.334 (2H, d, $J = 8$), 7.534−7.552 (3H, m), 8.026 (2H, d, $J = 8$), 8.133 (2H, d, $J = 8$), Anal. Calcd for $C_{15}H_{11}BrN_2O$: C, 57.16; H, 3.52; N. 8.89. Found: C, 57.04; H, 3.70; N, 8.96. IR (KBr): ν 631, 1610, 3018 cm^{-1}.

Synthesis of 9-4′-Bromobutylcarbazole (d). NaH (0.74 g, 0.020 mol) and 9H-carbazole (**b**) (3.34 g, 0.020 mol) were added to 100 mL of anhydrous *N*,*N*-dimethylformamide (DMF) in a 250 mL flask; the solution became clear after 1 h, and 3.0 mL (0.022 mol) of 1,4-dibromobutane was added dropwise. The reaction mixture was stirred for another 6 h and then poured into 300 mL of cool water; the organic components were extracted with CH_2Cl_2 (3 × 50 mL). The organic phase was washed with water and dried over anhydrous sodium sulfate. After the solvent was removed by rotary evaporation, the residue was purified by silica gel column chromatography with petroleum ether and acetic acid ethyl ester (v/v

(5) (a) Kwong, R. C.; Sibley, S.; Dubovoy, T.; Baldo, M.; Forrest, S. R.; Thompson, M. E. *Chem. Mater.* **1999**, *11*, 3709. (b) Chan, S. C.; Chan, M. C. W.; Wang, Y.; Che, C.-M.; Cheung, K. K.; Zhu, N. *Chem.—Eur. J.* **2001**, *7*, 4180. (c) Lu, W.; Mi, B.-X.; Chan, C. W. Hui, Z.; Zhu, N.; Lee, S.-T.; Che, C.-M. *Chem. Commun.* **2002**, 206. (d) Chang, S.-Y.; Kavitha, J.; Li, S.-W.; Hsu, C.-S.; Chi, Y.; Yeh, Y.-S.; Chou, P.-T.; Lee, G.-H.; Carty, A. J.; Tao, Y.-T.; Chien, C.-H. *Inorg. Chem.* **2006**, *45*, 137. (e) Zhuang, W.; Zhang, Y.; Hou, Q.; Wang, L.; Cao, Y. *J. Polym. Sci., Part A: Polym. Chem.* **2006**, *44*, 4174.

(6) (a) Gong, X.; Ng, P. K.; Chan, W. K. *Adv. Mater.* **1998**, *10*, 1337. (b) Li, Y.; Liu, Y.; Guo, J.; Wu, F.; Tian, W.; Li, B.; Wang, Y. *Synth. Met.* **2001**, *118*, 175. (c) Fu, C.; Li, M,; Su, Z.; Hong, Z.; Li, W.; Li, B. *Appl. Phys. Lett.* **2006**, *88*, 093507. (d) Li, F.; Cheng, G.; Zhao, Y.; Feng, J.; Liu, S.; Zhang, M.; Ma, Y.; Shen, J. *Appl. Phys. Lett.* **2003**, *83*, 4716. (e) Ley, K. D.; Whittle, C. E.; Bartberger, M. D.; Schanze, K. S. *J. Am. Chem. Soc.* **1997**, *119*, 3423.

(7) (a) Yam, V. W. W.; Li, B.; Yang, Y.; Chu, B. W. K.; Wong, K. M. C.; Cheung, K. K. *Eur. J. Inorg. Chem.* **2003**, *25*, 4035. (b) Wang, K.; Huang, L.; Gao. L.; Jin, L.; Huang, C. *Inorg. Chem.* **2002**, *41*, 3353. (c) Li, B.; Li, M.: Hong, Z.; Li, W.; Yu, T.; Wei, H. *Appl. Phys. Lett.* **2004**, *85*, 4786.

(8) (a) Li, Y.; Wang, Y.; Zhang, Y.; Wu, Y.; Shen, J. *Synth. Met.* **1999**, *99*, 257. (b) David, G.; Walsh, P. J.; Gordon, K. C. *Chem. Phys. Lett.* **2004**, *383*, 292.

(9) Li, F.; Zhang, M.; Cheng, G.; Feng, J.; Zhao, Y.; Ma, Y.; Liu, S.; Shen, J. *App. Phys. Lett.* **2004**, *84*, 148.

(10) (a) Li, F.; Zhang, M.; Feng, J.; Cheng, G.; Wu, Z.; Ma, Y.; Liu, S. *Appl. Phys. Lett.* **2003**, *83*, 365. (b) Chan, W. K.; Ng, P. K.; Gong, X.; Hou, S. *Appl. Phys. Lett.* **1999**, *75*, 3920.

(11) Peng, Z.; Bao, Z.; Galvin, M. E. *Adv. Mater.* **1998**, *10*, 680.

(12) Brunner, K.; Dijken, A. V.; Bötner, H.; Bastiaansen, J. J. A. M.; Kiggen, N. M. M.; Langeveld, B. M. W. *J. Am. Chem. Soc.* **2004**, *126*, 6035.

(13) Liang, F.; Zhou, Q.; Cheng, Y.; Wang, L.; Ma, D.; Jing, X.; Wang, F. *Chem. Mater.* **2003**, *15*, 1935.

(14) Yam, V. W. W.; Yang, Y.; Zhang, J.; Chu, B. W. K.; Zhu, N. *Organometallics* **2001**, *20*, 4911.

= 10: 1) to yield 3.00 g white needle crystals. ^{1}H NMR ($CDCl_3$, 500 MHz): δ 1.91 (m, 2H), 2.05 (m, 2H), 3.37 (t, 2H), 4.34 (t, 2H), 7.23 (m, 2H,), 7.38 (d, 2H, J = 8.0 Hz), 7.46 (t, 2H), 8.09 (d, 2H, J = 8.0 Hz). Anal. Calcd for $C_{16}H_{16}BrN$: C, 63.59; H, 5.34; N, 4.63. Found: C, 63.45; H, 5.28; N, 4.74. IR (KBr): ν 3048, 2935, 2858, 1587, 1450, 1370 cm^{-1}.

Synthesis of L1. NaH (0.37 g, 0.01 mol) and 2-pyridinylbenzoimidazole (1.95 g, 0.01 mol) were added to 100 mL of stirring anhydrous DMF in a 250 mL flask; 3.45 g (0.011 mol) of 2-(4-bromomethylphenyl)-5-phenyl-1,3,4-oxadiazole was added when the solution was clear. The mixture was stirred for 24 h, and then it was poured into 300 mL of cool water. The resulting white powder was collected by filtration and purified by silica gel column chromatography with petroleum ether and acetic acid ethyl ester (v/v = 10:1) to yield 2.10 g of yellow powder (60%). ^{1}H NMR ($CDCl_3$, 500 MHz): δ 6.299 (2H, s), 7.364 (6H, m), 7.553 (3H, m), 7.875 (1H, t, J = 8), 7.909 (1H, d, J = 8), 8.045 (2H, d, J = 8), 8.115 (2H, d, J = 6.5), 8.469 (1H, d, J = 7.5), 8.629 (1H, d, J = 3.5) Anal. Calcd for $C_{27}H_{19}N_5O$: C, 75.51; H, 4.46; N, 16.31. Found: C, 75.60; H, 4.52; N, 16.20. IR (KBr): ν 1446, 1549, 1770 cm^{-1}.

Synthesis of L2. The procedure was similar to that of compound **5**. Yield: 55%.^{1}H NMR ($CDCl_3$, 500 MHz): δ 2.016 (4H, m, J = 6.5), 4.340 (2H, t, J = 6.5), 4.846 (2H, t, J = 6.5), 7.240−7.343 (8H, m), 7.448−7.477 (2H, m), 7.828−7.888 (2H, m), 8.114 (2H, d, J = 7.5), 8.408 (1H, d, J = 8), 8.560 (1H, d, J = 4). Anal. Calcd for $C_{28}H_{24}N_4$: C, 80.74; H, 5.81; N, 13.45. Found: C, 80.89; H, 6.00; N, 13.11. IR (KBr): ν 3046, 2924, 1584, 1446, 1390 cm^{-1}.

Synthesis of 1. L1 (0.09 g, 0.210 mmol) and $Re(CO)_5Br$ (0.08 g, 0.200 mmol) were refluxed in 15 mL of toluene for 6 h. After the mixture was cooled to RT, the solvent was removed in a water bath under reduced pressure. The resulting yellow solid was purified by silica gel column chromatography with acetic acid ethyl ester and dichloromethane (v/v = 10:1). Yield: 0.124 g (80%). ^{1}H NMR ($CDCl_3$, 500 MHz): δ 5.994 (2H, s), 7.319−7.333 (3H, d, J = 7), 7.513−7.652 (7H, m), 7.838 (2H, d, J = 7.5), 7.939 (1H, m,), 8.098 (2H, d, J = 7.5), 8.180 (2H, d, J = 33.5), 8.196 (1H, d, J = 13), 9.238 (1H, d, J = 5.5). Anal. Calcd for $C_{30}H_{19}BrN_5O_4Re$: C, 46.22; H, 2.46; N, 8.98. Found: C, 46.22; H, 2.44; N, 9.10. IR (KBr): ν 2018, 1898 cm^{-1}.

Synthesis of 2. The procedure is similar to that of **1**. The yellow solid was purified by silica gel column chromatography with dichloromethane and THF. Yield: 80%. ^{1}H NMR ($CDCl_3$, 500 MHz): δ 1.979 (2H, m), 2.148 (2H, m), 4.335 (2H, t, J = 7.5), 4.417 (2H, t, J = 7.5), 7.133 (2H, d, J = 8.5), 7.277 (2H, d, J = 8), 7.376 (2H, d, J = 8), 7.463 (4H, t, J = 8), 7.525 (1H, t, J = 7), 7.636 (1H, d, J = 8), 7.727 (1H, d, J = 8), 8.051 (1H, d, J = 7.5), 8.119 (2H, d, J = 7.5). Anal. Calcd for $C_{31}H_{24}BrN_4O_3Re$: C, 48.57; H, 3.16; N, 7.31. Found: C, 48.30; H, 3.31; N, 7.20. IR (KBr): ν 2019, 1897 cm^{-1}.

Spectroscopy. The IR spectra were acquired using a Magna560 FT-IR spectrophotometer. Element analyses were performed using a Vario Element Analyzer. ^{1}H NMR spectra were obtained using a Bruker AVANCE 500 MHz spectrometer with tetramethylsilane as the internal standard. A suitable amount of sample for emission studies was dissolved in the appropriate solvent to make the concentration 10^{-5} mol/L, and the absorbance of the solution was measured. This concentration provided enough material for data acquisition but excluded self-quenching processes. The corrected PL spectra of the degassed solution were collected by a Shimadzu RF-5301PC spectrophotometer. The luminescence quantum yields were measured by comparison of the fluorescence intensities (integrated areas) of a standard sample (quinine sulfate) and the unknown sample according to the equation

$$\Phi_{unk} = \Phi_{std}(I_{unk}/A_{unk})(A_{std}/I_{std})(\eta_{unk}/\eta_{std})^2$$

where Φ_{unk} is the luminescence quantum yield of the sample, Φ_{std} is the luminescence quantum yield of quinine sulfate and is taken as 0.546,[15] I_{unk} and I_{std} are the integrated fluorescence intensities of the unknown sample and quinine sulfate, respectively, and A_{unk} and A_{std} are the absorbances of the unknown sample and quinine sulfate at excitation wavelengths of 420 nm for **1** and 364 nm for quinine sulfate and **2**. The η_{unk} and η_{std} terms represent the refractive indices of the corresponding solvents (pure solvents were assumed). The excited-state lifetimes were detected by a system equipped with a TDS 3052 digital phosphor oscilloscope pulsed Nd:YAG laser with a THG 355 nm output and a computer-controlled digitizing oscilloscope according to the reported method.[16] The Origin 7.0 program by OriginLab Corporation was used for the curve-fitting analysis.

Crystallography. Yellowish single crystals of complexes **2** suitable for X-ray diffraction studies were grown from slow evaporation of a CH_2Cl_2 solution. The crystals were measured on a Bruker Smart Apex CCD single-crystal diffractometer using λ-(Mo KR) radiation, 0.7107 Å at 293 K. An empirical absorption was based on the symmetry-equivalent reflections and applied to the data using the SADABS program. The structure was solved using the SHELXL-97 program.[17] The crystallographic refinement parameters of **2** are summarized in Table 1, while the selected bond distances and angles are given in Table 2.

Thermal Analysis. Thermogravimetric analysis (TGA) was performed on ~2 mg of **1** and **2** using a Perkin-Elmer thermal analyzer. The samples were dried under vacuum at 56.5 °C before being heated from 40 to 605 °C at a heating rate of 10.0 °C/min. A 10 mL/min flow of dry nitrogen was used to purge the sample at all times.

Cyclic Voltammetry. Cyclic voltammetry measurements were conducted on a voltammetric analyzer (CH Instruments, Model 620B) with a polished Pt plate as the working electrode, Pt mesh as the counter electrode, and a commercially available saturated calomel electrode (SEC) as the reference electrode at a scan rate of 0.1 V/s. The voltammograms were recorded using CH_3CN sample solutions with ~10^{-3} M **1** and **2** and 0.1 M ammonium hexafluorophosphate (AHFP) as the supporting electrolyte. Prior to each electrochemical measurement, the solution was purged with nitrogen for ~10−15 min to remove the dissolved O_2 gas.

Fabrication of EL Devices. Prepatterned ITO substrates with a resistivity of <30 Ω and an effective individual device area of 4 mm^2 were cleaned by sonication in detergent solution, water, and ethanol, sequentially. After they were blown dry with nitrogen, the ITO substrates were treated with oxygen plasma for 1 min before being loaded into the vacuum chamber. All layers in the diodes are deposited by a resistive heating method. The pressure of the chamber is below 3×10^{-4} Pa. LiF (0.8 nm) was deposited as the electron-injection layer, which was capped with 200 nm of Al as the cathode. The EL spectra and Commission Internationale de L'Eclairage (CIE) coordinates of the devices were measured by a

(15) Ye, K.; Wang, J.; Sun, H.; Liu, Y.; Mu, Z.; Li, F.; Jiang, S.; Zhang, J.; Zhang, H.; Wang, Y.; Che, C.-M. *J. Phys. Chem. B* **2005**, *109*, 8008.

(16) Villegas, J. M.; Stoyanov, S. R.; Rillema, D. P. *Inorg. Chem.* **2002**, *41*, 6688.

(17) Sheldrick, G. M. *SHELXTL*, version 5.10; Siemens Analytical X-ray Instruments Inc.: Madison, WI, 1998. (b) *SMART* and *SAINT*; Siemens Analytical X-ray Instruments Inc.: Madison, WI, 1995. (c) Sheldrick, G. M. *SADABS*; University of Göttingen: Göttingen, Germany, 1996.

Table 1. Crystal Data for **2**·CH_2Cl_2

formula	$C_{32}H_{26}Cl_2N_4O_3ReBr$
fw	851.58
T (K)	293(2)
wavelength (Å)	0.71073
cryst syst	monoclinic
space group	$P2_1/n$
a (Å)	14.7407(8)
b (Å)	9.1414(5)
c (Å)	23.4181(13)
α (deg)	90
β (deg)	98.2320(10)
γ (deg)	90
V (Å^3)	3123.1(3)
Z	4
ρ_{calcd} (Mg/m^3)	1.811
μ (mm^{-1})	5.381
F(000) (e)	1656
cryst color	yellow
cryst size (mm)	0.311× 0.287 × 0.193
range of transm factors (deg)	1.54−28.24
reflns collected	18 724
unique	7347
completeness to $\theta = 28.24$	95.10%
data/restraints/params	7347/0/415
GOF on F^2	1.065
R1, wR2 [$I > 2\sigma(I)$]	0.0636, 0.1483
R1, wR2 (all data)	0.1166, 0.1713

Table 2. Selected Bond Bengths (Å) and Angles (deg) for **2**·CH_2Cl_2

C(1)−Re(1)	1.863(13)	N(1)−Re(1)	2.149(7)
C(2)−Re(1)	1.994(11)	N(2)−Re(1)	2.195(8)
C(3)−Re(1)	1.904(11)	Br(1)−Re(1)	2.5956(12)
C(9)−N(1)	1.322(10)	C(8)−N(2)	1.338(11)
O(1)−C(1)−Re(1)	177.1(11)	C(1)−Re(1)−N(2)	170.3(4)
O(2)−C(2)−Re(1)	174.7(13)	C(2)−Re(1)−N(2)	93.6(4)
O(3)−C(3)−Re(1)	178.0(10)	C(3)−Re(1)−N(1)	168.7(4)
C(9)−N(1)−Re(1)	117.8(6)	C(1)−Re(1)−N(1)	99.7(4)
C(10)−N(1)−Re(1)	133.9(6)	C(2)−Re(1)−N(1)	96.9(3)
C(8)−N(2)−Re(1)	119.0(6)	N(1)−Re(1)−N(2)	72.7(3)
C(4)−N(2)−Re(1)	122.5(7)	C(3)−Re(1)−Br(1)	92.2(3)
C(1)−Re(1)−C(3)	90.0(5)	C(1)−Re(1)−Br(1)	88.2(4)
C(3)−Re(1)−C(2)	88.3(4)	C(2)−Re(1)−Br(1)	178.4(3)
C(1)−Re(1)−C(2)	93.3(5)	N(1)−Re(1)−Br(1)	82.38(18)
C(3)−Re(1)−N(2)	97.0(4)	N(2)−Re(1)−Br(1)	84.85(18)

PR650 spectrometer. All measurements were carried out at RT under ambient conditions.

Results and Discussion

Synthesis and Characterization. Ligands **L1** and **L2** and the corresponding rhenium(I) complexes **1** and **2** were prepared according to literature methods, and their structures are shown in Scheme 1. The purity and composition of the complexes were confirmed by ^{1}H NMR, IR, and elemental analyses. The ^{1}H NMR spectra of complexes **1** and **2** have some differences with those of corresponding free diimine ligands **L1** and **L2**. Compared to the free ligands, these signals were shifted toward low field because of the formation of new coordination bonds between the synthesized ligands and the Re metal centers.[18]

Structure of 2·CH_2Cl_2. Using the single-crystal X-ray diffraction method, we obtained solid evidence to support the structure of **2**·CH_2Cl_2. An ORTEP diagram of **2** is shown in Figure 1, and the crystal data are presented in Table 1; selected bond distances and angles for the complexes are listed in Table 2. The coordination geometry at the Re atom is a distorted octahedron with the three carbonyl ligands arranged in a facial fashion. The distances of C(1), C(2), and C(3) to Re(1) are 1.863(13), 1.994(11), and 1.904(11) Å, respectively, and the average Re−N bond distance is 2.175 (8) Å. The C−C bond distance for the bridgehead carbon atoms of **L2** (C(8)−C(9)) is 1.464 (12) Å, which is in agreement with that for the 2-pyridinylbenzoimidazole (Pybm) congener.[7b] The bond angles in Table 2 clearly indicate that the CO ligands are linearly coordinated. The bond angles between adjacent CO carbon atoms are 88.3(5)−93.3(5)°, which is close to 90°, but the bond angle between the coordinated nitrogen atoms of ligand **L2** is 72.7(3)°, which is much less than 90°. This is not only a result of the steric requirement of the bidentate coordination of **L2** but also the result ofa twist of the imidazole ring relative to the pyridine plane. This twist is clearly verified by the fact that the plane of the pyridine ring intersects that of the imidazole ring at an angle of 5.0° in normal. C(1) is constrained to be isotropic because of its disorder in the crystals formed at RT. All other bond distances and angles are comparable to those found for the related Re(I) complexes.[19]

Thermal Analysis. TGA was performed on complexes **1** and **2** in a N_2 atmosphere to investigate their stable characteristics, and the TGA traces of **1** and **2** are presented in Figure 2. Complex **1** began to lose weight when it was heated to 328 °C, which should be attributed to the loss of the bromine anion and carbonyl groups. **L1** began to dramatically disassociate or sublimate at 487 °C and totally decomposed at 600 °C. Complex **2** shows thermal characteristics similar to those of **1** in a N_2 atmosphere: it began to decompose gradually at 365 °C probably because of the loss of the carbonyl groups and bromine anion. At temperatures higher than 457 °C, the weight loss is probably caused by the unassisted thermolysis of **L2** or simply its sublimation. This process finished at 550 °C. Therefore, both **1** and **2** are stable enough to be sublimated to construct OLED devices at ∼300 °C.

Electrochemistry. Cyclic voltammograms of complexes **1** and **2** are shown in Figure 3 and exhibit irreversible metal-centered oxidation and ligand-based reduction in CH_3CN solution, which are consistent with the redox behavior of Pybm-based Re(I) diimine complexes reported in the literature.[7b] Complex **1** shows irreversible anodic waves at $V_{1/2} = +1.26$ V with an onset oxidation potential of +1.19 V vs SCE and irreversible cathodic waves at $E_{1/2} = -1.50$ V with an onset reduction potential of −1.20 V vs SCE. The anodic waves are associated with a Re^I-based oxidation process (Re^I/Re^{II}), and the cathodic waves are associated with a ligand-based reduction process ($[Re^ICl(CO)_3(L)]/ [Re^ICl(CO)_3(L^•)]^-$).[20]

(18) Zhang, M.; Lu, P.; Wang, X.; He, L.; Xia, H.; Zhang, W.; Yang, B.; Liu, L.; Yang, L.; Yang, M.; Ma, Y.; Feng, J.; Wang, D.; Tamai, N. *J. Phys. Chem. B* **2004**, *108*, 13185.

(19) Rajendran, T.; Manimaran, B.; Lee, F. Y.; Lee, G. H.; Peng, S. M.; Wang, C. C.; Lu, K. L. *Inorg. Chem.* **2000**, *39*, 2016.

(20) (a) Berger, S.; Klein, A.; Kaim, W.; Fiedler, J. *Inorg. Chem.* **1998**, *37*, 5664. (b) Moya, S. A.; Guerrero, J.; Pastene, R.; Schmidt, R. Sariego, R. *Inorg. Chem.* **1994**, *33*, 2341.

Scheme 1. Synthetic Route to Complexes **1** and **2**[a]

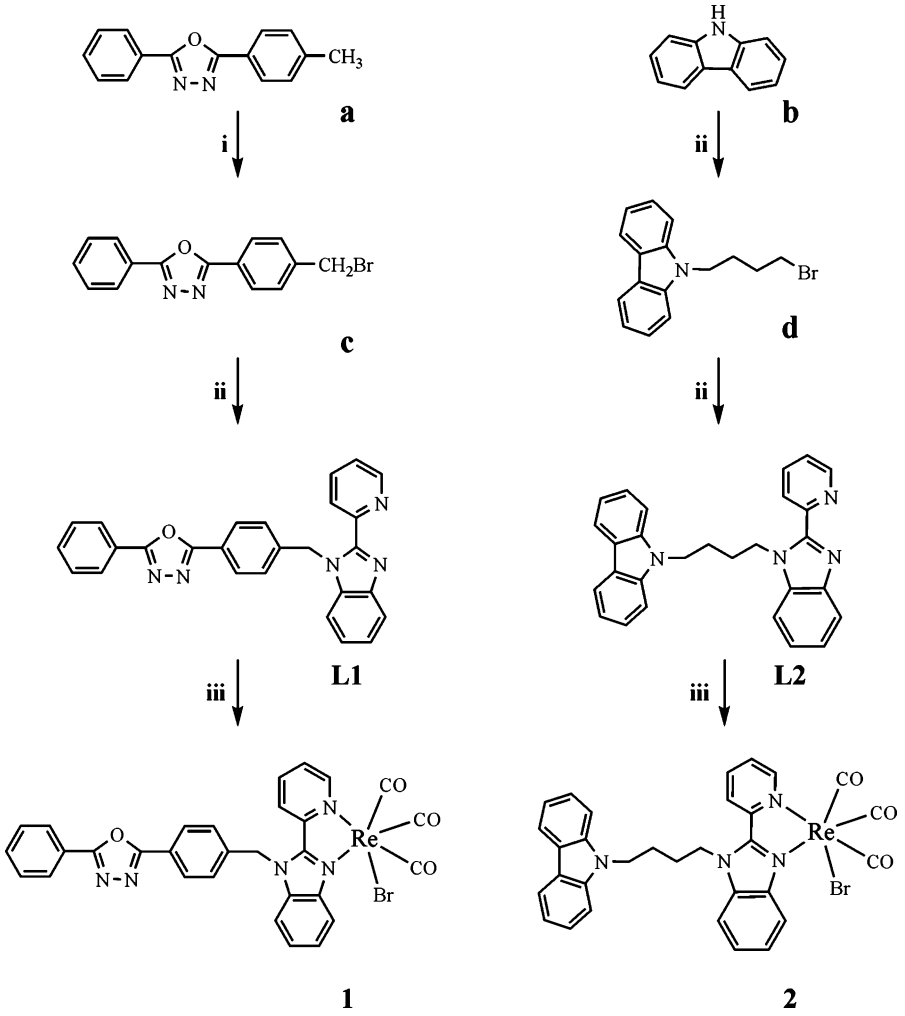

[a] (i) NBS, BPO, CCL_4, 120 °C; (ii) NaH, DMF, RT; (iii) $Re(CO)_5Br$, toluene, 80 °C.

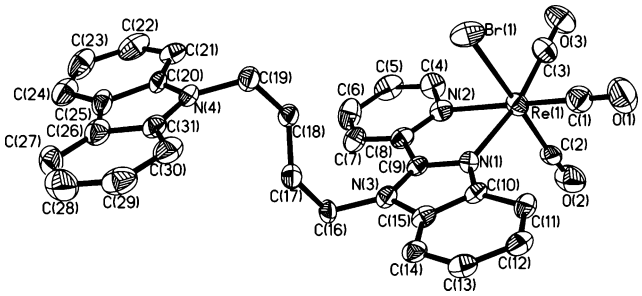

Figure 1. ORTEP drawing of a crystal of **2** with displacement ellipsoids at the 30% probability level.

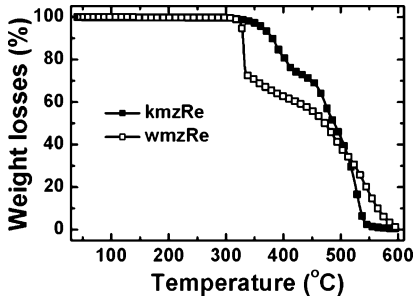

Figure 2. TGA traces for complexes **1** and **2**.

Complex **2** shows a similar redox behavior. The energy levels of the highest-occupied molecular orbital (HOMO) and the lowest-unoccupied molecular orbital (LUMO) are calculated from the onset oxidation (E_{onset}(Ox)) and reduction (E_{onset}(Red)) potentials with the formula $E_{HOMO} = -4.74 - E_{onset}$(Ox) (−4.74 V for SCE with respect to the zero vacuum level[21] and E_{onset}(Ox) = +1.07 V for **2**) and $E_{LUMO} = -4.74 - E_{onset}$(Red) ($E_{onset}$(Red) = −1.30 V for **2**). These calculations give HOMO and LUMO energy levels of −5.93 and −5.81 eV and −3.54 and −3.44 eV for **1** and **2**, respectively. The gaps between the LUMO and the HOMO energy levels of **1** and **2** were thus determined to be 2.39 and 2.37 eV, respectively, which are in good agreement with those (2.38 eV) obtained from UV−vis spectroscopy. The electron affinity of −2.55 eV for 2,5-diphenyl-1,3,4-oxadiazole and the ionization potential of −5.78 eV for carbazole indicate they possess electron- and hole-transporting abilities, respectively. As a result, the introduction of them into the parent complex (Pybm)$Re(CO)_3Br$ (E_{LUMO} = −3.47 eV,

(21) (a) Bard, A. J.; Faulkner, L. R. *Electrochemical Methods Fundamental and Applications*; Wiley: New York, 1980. (b) Wu, D. G.; Huang, C. H.; Gan, L. B.; Zheng, J.; Huang, Y. Y.; Zhang, W. *Langmuir* **1999**, *15*, 7276. (c) Ashwini, K. A.; Samson, A. J. *Chem. Mater.* **1996**, *8*, 579.

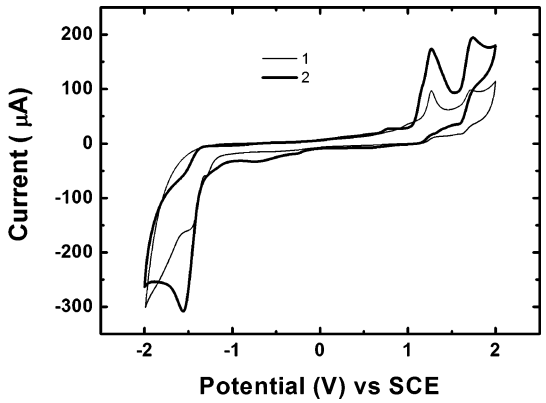

Figure 3. Cyclic voltammograms of complexes **1** and **2** measured in CH_3CN (vs SCE) at a scan rate of 0.1V/s. A polished Pt plate and a Pt mesh were used as the working electrode and the counter electrode, respectively. AHFP was taken as supporting electrolyte.

Table 3. Absorption and Emission Spectral Data of **1** and **2** in CH_2Cl_2 and the Solid State at 293 K

			excitation	emission	
complex	medium	abs [λ, nm (ϵ, $\times 10^{-3}$ mol^{-1}cm^{-1})]	λ (nm)	λ_{max} (nm)	ϕ (degass)
1	CH_2Cl_2	284 (41.6), 340 (22.8), 420 (4.7)	379, 420	601	2.6×10^{-3}
	solid		420, 468	569	
2	CH_2Cl_2	260 (40.9), 292 (30.9), 328 (27.2), 340 (25.4), 366 (6.4)	276, 370, 415	577	3.1×10^{-3}
	solid		252, 282, 436	536	

$E_{HOMO} = -5.84$ eV) makes the difference in the redox potentials of the Re(I)−Re(II) couples between **1** and **2,** suggesting that the property of the functional group affects the stability of the metal orbital energy levels.

Photophysical Properties. The absorption and emission spectral data for **1** and **2** along with lifetimes and emission quantum yields in deoxygenated dichloromethane at 293 K are summarized in Table 3. Figure 4a shows UV−vis absorption spectra and excitation spectra of complexes **1** and **2** in dichloromethane. For both **1** and **2**, the dominant absorption bands in the 260−360 nm region were assigned to an admixture of intraligand ($\pi \rightarrow \pi^*$ (L)) transitions of the carrier-transporting moieties and the Pybm moiety. These assignments were based on the absorption spectra of the free ligands shown in Figure S1 (in the Supporting Information) and similar Re(I) complexes.[22] These bands are also accompanied by lower-energy features extending into the visible region from 360 to 520 nm which are tentatively assigned to the metal-to-ligand charge-transfer dπ(Re) $\rightarrow$ π^*(N−N) (MLCT) transitions. It is obvious that all of the MLCT absorption bands of complexes **1** and **2** are similar to those observed in the related Re(I) complexes and show little difference from each other which may be caused by the weak MLCT transition absorbance.

Figure 4b exhibits the emission spectra of complexes **1**, **2**, and (2-pyridinylbenzoimidazole)$Re(CO)_3Br$ [(Pybm)$Re(CO)_3Br$] in dichloromethane. The broad PL spectra in CH_2Cl_2 solution only show the ^{3}MLCT transition bands with maximum values of 601 nm for **1** and 577 nm for **2**, which implies that the effects of the 2,5-diphenyl-1,3,4-oxadiazole and carbazole groups on the energy level of the π^* orbital of the parent complex (Pybm)$Re(CO)_3Br$ are different. It was reported that the effects should be as follows: the energy of the π^* orbital is lowered by the presence of an electron-withdrawing moiety (2,5-diphenyl-1,3,4-oxadiazole) and heightened by the introduction of an electron-donating moiety (carbazole).[6a] These effects are also verified by the difference of the excitation spectra of **1** and **2** in CH_2Cl_2 solution: the broad and low-energy MLCT band in the absorption spectra partially resolves into two bands in the scanning excitation spectrum, namely, the ^{1}MLCT and ^{3}MLCT states at 379 and 420 nm and 370 and 415 nm for **1** and **2**, respectively. As can be seen from Figure 4b, the PL spectra of (Pybm)$Re(CO)_3Br$ and complex 2 are almost the same, indicating the effect of carbazole group on the energy of π^* orbital is negligible in complex **2**, which should be attributed to the longer distance (5.38 Å) between the carbazole and (Pybm)$Re(CO)_3Br$ moieties.

Excitation at either the $\pi \rightarrow \pi^*$ absorption region ($\sim$280 nm) or the MLCT absorption region ($\sim$370 nm) leads to the same MLCT emission ($\sim$578 nm) at RT for **2**, which indicates there is potential surface crossing from the higher $\pi \rightarrow \pi^*$ state to the lower MLCT state, and the major contribution of the observed emission is from the MLCT state.[23] However, the same potential surface crossing does not exist for **1** because the excitation spectrum of **1** in CH_2Cl_2, measured by monitoring the emission λ_{max} at RT, did not show the $\pi \rightarrow \pi^*$ excitation band probably because of the lower emission energy of the ligand **L1** shown in Figure S1. This character of the photoluminescence is further revealed by the measurement of the excited-state lifetimes. As indicated in Figure 5, the PL spectrum of complex **2** is composed of two exponential decays with lifetimes of $\tau_1 = 0.91$ μs ($A_1 = 0.25$) and $\tau_2 = 0.22$ μs ($A_2 = 7.25$).[24] In general, if there is potential surface crossing from the higher ligand $\pi \rightarrow \pi^*$ state to the lower MLCT state, one can expect, on the basis of the energy gap law, a shorter decay lifetime from the $\pi \rightarrow \pi^*$ state than the lower MLCT state.[25] However, the potential surface crossing for **2** from the higher $\pi \rightarrow \pi^*$ state to the MLCT state is not efficient. Therefore, the assignment of the major, short-lived decay component to emission from the ^{3}MLCT state and the minor, long-lived component to the emission from the $\pi \rightarrow \pi^*$ state should be reasonable. Complex **1** also exhibits a biexponential decay pattern with lifetimes of $\tau_1 = 0.41$ μs ($A_1 = 1.00$) and $\tau_2 = 0.12$ μs ($A_2 = 1139.70$), confirming there is hardly any potential surface crossing for **1** from $\pi \rightarrow \pi^*$ state to the

(22) (a) Lo, K. K.-W.; Lau, J. S.-Y.; Fong, V. W.-Y.; Zhu, N. *Organometallics* **2004**, *23*, 1098. (b) Guerrero, J.; Piro, O. E.; Wolcan, E.; Feliz, M. R.; Ferraudi, G.; Moya, S. A. *Organometallics* **2001**, *20*, 2842.

(23) Sacksteder, L.; Zipp, A. P.; Brown, E. A.; Streich. J.; Demas, J. N.; DeGraff, B. A. *Inorg. Chem.* **1990**, *29*, 4335.

(24) Ranjan, S.; Lin, S.-Y.; Hwang, K. C.; Chi, Y.; Ching, W.-L.; Liu, C.-S.; Tao, Y.-T.; Chien, C.-H.; Peng, S.-M.; Lee, G.-H. *Inorg. Chem.* **2003**, *42*, 1248.

(25) (a) Shaw, J. R.; Schmehl, R. H. *J. Am. Chem. Soc.* **1991**, *113*, 389. (b) Wallace, L.; Rillema, D. P. Inorg. Chem. **1993**, *32*, 3836. (c) Striplin, D. R.; Crossby, G. A. *Coord. Chem. Rev.* **2001**, *211*, 163.

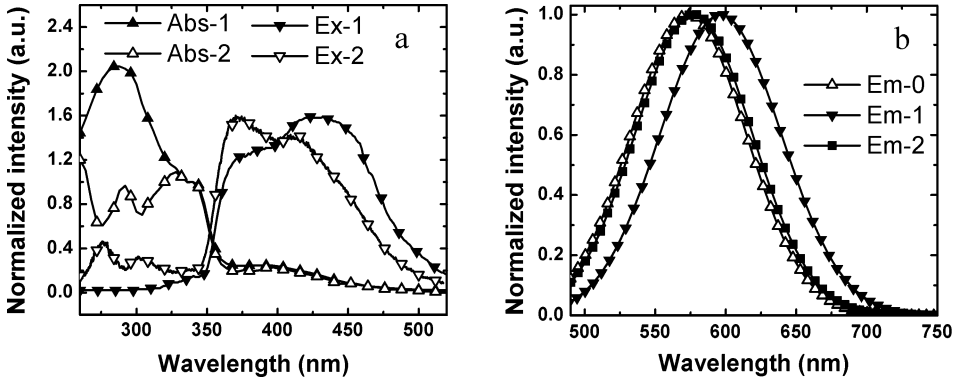

Figure 4. (a) UV−vis absorption spectra and excitation spectra of complexes **1** and **2** in CH_2Cl_2 solution. (b) Emission spectra of complexes **1**, **2**, and (Pybm)Re(CO)$_3$Br (0) in CH_2Cl_2 solution.

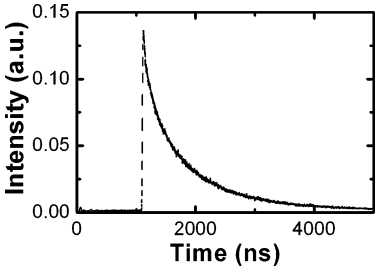

Figure 5. Photoluminescence lifetime decay measurement of the solid thin film of complex **2**.

MLCT state. Finally, the luminescence quantum yields in deaerated dichloromethane were measured to be 2.6×10^{-3} and 3.1×10^{-3} for complexes **1** and **2**, respectively.

EL Properties. The OLEDs with complexes **1** and **2** as dopants in the CBP emissive layer were fabricated with the structure ITO/*m*-MTDATA (30 nm)/NPB (20 nm)/dopant: CBP($\times$ wt %, 30 nm)/Bphen (20 nm)/Alq_3 (20 nm)/LiF (0.8 nm)/Al (200 nm).[9a] *m*-MTDATA is used as the hole-injection layer; NPB is the hole-transporting and electron-blocking layer, and Bphen and Alq_3 are employed as the exciton-blocking layer and the electron-transporting layer, respectively. Carrier recombination occurring in the CBP layer is necessary to generate CBP excitons. The Bath layer with a LUMO level of −2.4 eV and the NPB layer with a HOMO level of −5.2 eV pave the ways for electrons and holes to transport from Alq_3 (LUMO level = −3.1 eV) and *m*-MTDATA (HOMO = −5.1 eV) to the CBP layer (HOMO = −5.5 eV, and LUMO = −2.0 eV), respectively. Because the PL spectrum of CBP centered at 380 nm shows large spectral overlap with the MLCT absorption bands of complexes **1** and **2**, there should exist efficient Föster-type energy transfer in the constructed light-emitting devices, which can emit stable white light at a suitable doped concentration. To study the effect of the functional groups on the performance of the electrophosphoresent devices based on Re(I) complexes, the EL properties of **1**- and **2**-based devices are reported in this article. The key parameters of the OLEDs based on (Pybm)Re(CO)$_3$Br, **1**, and **2** are listed in the Table 4.

Figure 6 shows the EL spectra for the devices based on **1** and **2** at an applied voltage of 13 V. The EL emission band centered at 410 nm originates from CBP. The lower-energy

Table 4. Key Parameters of the OLEDs Based on Complexes **1** and 2 and (Pybm)Re(CO)$_3$Br

complexes	B_{max}[a] (cd/m^2)	λ_{max}[b] (nm)	η_{max}[c] (cd/A)
1	1774	∼*590*	0.53
2	2300	∼*570*	1.60
(Pybm)Re(CO)$_3$Br	1240	∼*564*	0.75

[a] The maximum brightness. [b] The maximum EL emission wavelength. [c] The maximum current efficiency.

emission bands attributed to the ^{3}MLCT emission from the Re(I) complexes show red shifts from 572 to 600 nm for **1** and from 568 to 588 nm for **2**, accompanying the decrease of the emission from CBP with the increase of the doping concentration from 6 to 20 wt %. The difference of the EL emission from Re(I) complexes can also be attributed to the effect of the carrier-transporting groups as described above. The red shift should be explained by the interaction of the dopant molecules at higher doping concentration.[26] When the doping concentration of **1** and **2** is higher than 10 wt %, the emission from CBP almost disappears, and the EL spectra only demonstrate the broad emission bands centered at 600 nm for **1**-based devices and 588 nm for **2**-based ones. The CIE coordinates for the devices with 10 wt % **1** and **2** are $x = 0.519$ ($\pm$0.002), $y = 0.46$ ($\pm$0.002) from $J = 4.29$ to 381.68 mA/cm^2 and $x = 0.504$ (no shift), $y = 0.474$ ($\pm$0.003) from $J = 0.73$ to 476.86 mA/cm^2, respectively. The devices with 8 wt % **1** and **2** were found to be good WOLEDs which demonstrate CIE coordinates of (0.35, 0.32) at 11 V and (0.34, 0.33) at 15 V, respectively, both of which are close to those of pure white light (0.33, 0.33). These CIE coordinates also show minor shifts at different current densities. For **1**-based devices, the CIE coordinates show $\Delta x = \pm 0.02$, $\Delta y = \pm 0.04$ from $J = 7.14$ to 180.10 mA/cm^2, and for **2**-doped devices, the CIE coordinates show the same shifts from $J = 80.00$ to 372.14 mA/cm^2.

Figure 7 presents the luminance−voltage ($L-V$) characteristics of the devices based on **1** (a) and **2** (b) with doping concentrations of 6, 8, 10, 20 wt %. As can be observed, the maximum brightness achieved from the devices based on 8 wt % of complexes **1** and **2** reached 1774 cd/m^2 at 17 V and 2300 cd/m^2 at 16 V, respectively. The current−voltage

(26) Polleux, J.; Pinna, N.; Antonietti, M.; Niederberger, M. *Adv. Mater.* **2004**, *16*, 432.

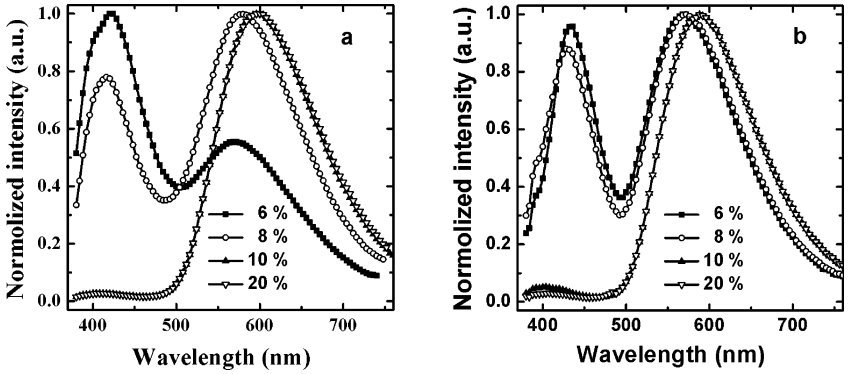

Figure 6. EL spectra of the OLEDs based on **1** (a) and **2** (b) at 13 V.

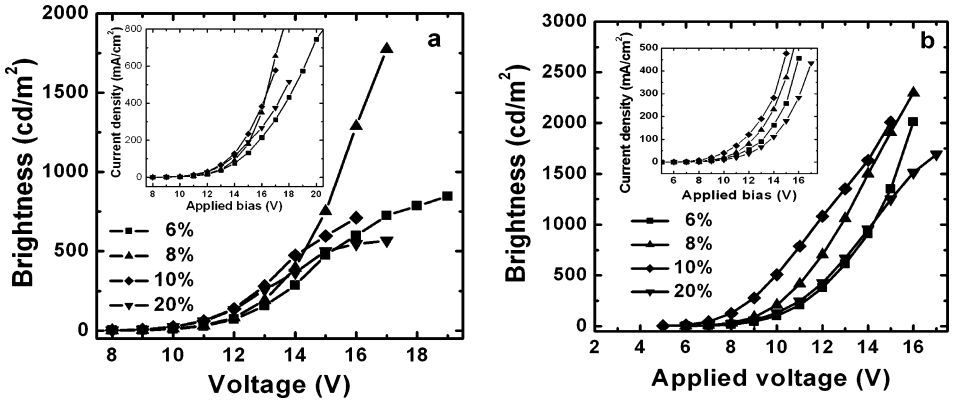

Figure 7. $L-V$ and $I-V$ (inset) characteristics of the OLEDs based on **1** (a) and **2** (b).

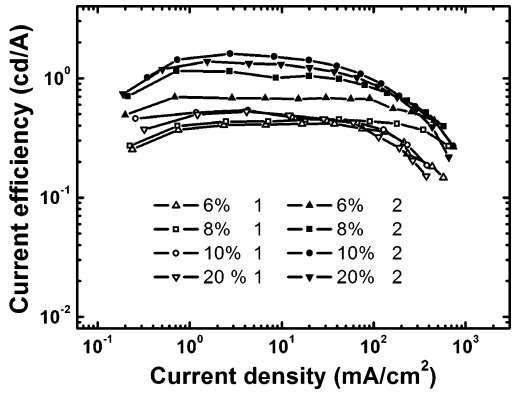

Figure 8. Current efficiency of the OLEDs based on **1** and **2** as a function of current density.

($I-V$) characteristics of these devices are also presented in the inset of Figure 7. When the doping concentration is not higher than 10 wt %, the current density at a given voltage increases with the doping concentration, indicating the good carrier-transporting ability of both **1** and **2** in the CBP emissive layer. The $I-V$ curves for the devices based on 20 wt % Re(I) complexes lie below the other $I-V$ curves, which may be caused by phase separation at higher doping concentration.

Figure 8 presents the characteristic of the EL efficiency−current density of the devices based on **1** and **2**. The efficiency of these devices decreases slowly at first with an increase of the current densities, suggesting that the saturation of the phosphorescence sites is not severe because of the steric hindrance effect of the functional groups in **1** and **2**. The saturation is responsible for the fast decrease of the EL efficiency at high current density, exceeding 300 mA/cm^2. The devices with a doping concentration of 10 wt % exhibit the maximum efficiency; the efficiency of **2**-based devices at 230 mA/cm^2 stays as high as 56% of the maximum value which appears at 2.7 mA/cm^2, and that of **1**-based devices at 230 mA/cm^2 is 51% of the maximum value at 4.2 mA/cm^2. These data suggest that the devices based on **1** and **2** not only exhibit excellent white emission but also are stable in a large current range.

As can be observed from the Table 4 and the Figure 8, the order of the maximum efficiency of the OLEDs is as follows: complex **2** > (Pybm)Re(CO)$_3$Br > complex **1**. The explanation might be that when (Pybm)Re(CO)$_3$Br is linked with the hole-transporting group of carbazole, the charge carrier injection balance in the devices are improved, resulting in the effective carrier recombination. In contrast, the introduction of the electron-transporting group of 2,5-diphenyl-1,3,4-oxadiazole into (Pybm)Re(CO)$_3$Br will lower the device's efficiency. It also implies that (Pybm)Re(CO)$_3$Br may possess effective electron-transporting and weak hole-transporting ability. Therefore, unlike other metal complexes,[13,27] modifying some Re(I) complexes with a suitable hole-transporting moiety would lead to a better carrier-injection and -transportation balance and, consequently, to the improvement of the device performances.

(27) Wang, J. F.; Wang, R. Y.; Yang, J.; Zheng, Z. P.; Carducci, M. D.; Cayou, T.; Peyghambarian, N.; Jabbour, G. E. *J. Am. Chem. Soc.* **2001**, *123*, 6179.

Summary

Rhenium(I) complexes **1** and **2** were successfully synthesized according to the molecular engineering, and they are stable enough to be sublimated during EL-device fabrication. The lifetime measurements confirmed that both **1** and **2** display biexponential phosphorescent emission with triplet excited-state lifetimes of 0.41 and 0.12 μs for **1** and 0.91 and 0.22 μs for **2**. When the doping concentration is 8 wt %, the devices demonstrate CIE coordinates of $x = 0.35$, $y = 0.32$ with a maximum brightness of 1774 cd/m^2 at 17 V for the electron-transporting group 2,5-diphenyl-1,3,4-oxadiazole-containing **1** and CIE coordinates of $x = 0.34$, $y = 0.33$ with a maximum brightness of 2300 cd/m^2 at 16 V for hole-transporting group carbazole-containing **2**. The performance of the devices based on **2** is notably superior to that of the complex **1**-based devices for a given doping level; it is believed that the modification of some diimine rhenium(I) carbonyl complexes with suitable hole-transporting moieties would lead to a better carrier-injection and -transportation balance and, consequently, to the improvement of the OLEDs' performances, and we are in the progress of exploring these possibilities.

Acknowledgment. The authors gratefully thank the One Hundred Talents Project from Chinese Academy of Sciences and the NSFC (Grant 20571071) for financial support.

Supporting Information Available: Figure showing the absorption spectra and PL spectra of ligands **L1** and **L2** and crystallographic data in CIF format. This material is available free of charge via the Internet at http://pubs.acs.org.

IC061645O